Vapor deposition of copper(I) bromide films via a two-step conversion process

Rachel Heasley[a)]
John A. Paulson School of Engineering and Applied Sciences, Harvard University, 29 Oxford Street, Cambridge, Massachusetts 02138

Christina M. Chang[a)] and Luke M. Davis
Department of Chemistry and Chemical Biology, Harvard University, 12 Oxford Street, Cambridge, Massachusetts 02138

Kathy Liu
Department of Chemistry and Chemical Biology, Harvard University, 12 Oxford Street, Cambridge, Massachusetts 02138 and Center for Excellence in Education, Research Science Institute, 8201 Greensboro Drive, Suite 215, McLean, Virginia 22102

Roy G. Gordon[b)]
John A. Paulson School of Engineering and Applied Sciences, Harvard University, 29 Oxford Street, Cambridge, Massachusetts 02138 and Department of Chemistry and Chemical Biology, Harvard University, 12 Oxford Street, Cambridge, Massachusetts 02138

(Received 5 September 2016; accepted 28 October 2016; published 9 November 2016)

Thin films of Cu_2S grown by pulsed-chemical vapor deposition of bis(*N*,*N*′-di-*sec*-butylacetamidinato)dicopper(I) and hydrogen sulfide were converted to CuBr upon exposure to anhydrous hydrogen bromide. X-ray diffraction shows that the as-deposited films have a polycrystalline Cu_2S structure. After exposure to HBr gas, the surface of the films is transformed to a γ-CuBr polycrystalline structure. Scanning electron microscopy and X-ray photoelectron spectroscopy reveal complete conversion of up to 100 nm of film. However, when the conversion to CuBr approaches the interface between as-deposited Cu_2S and the SiO_2 substrate, the morphology of the film changes from continuous and nanocrystalline to sparse and microcrystalline. © *2016 American Vacuum Society*. [http://dx.doi.org/10.1116/1.4967726]

I. INTRODUCTION

Research into photovoltaics employing a perovskite absorber layer [formula ABX_3, in which $A = CH_3NH_3^+$, $CH(NH_2)_2^+$; $B = Pb^{2+}$, Sn^{2+}; and $X = I^-$, Br^-, Cl^-] has seen dramatic growth in the past 7 years, yielding an increase in power conversion efficiency from 3.8% in 2009 (Ref. 1) to 22.1% in 2016.[2] One limiting factor in the commercial development of complete perovskite solar cells is the high cost of the hole-transport material (HTM).[3] The HTM is a p-type semiconductor layer that extracts positive charges (holes) from the perovskite absorber and transfers them to the back contact. Currently, the most efficient perovskite solar cells use the HTM 2,2′,7,7′-tetrakis(*N*,*N*-di-*p*-methoxyphenylamine)-9,9′-spirobifluorene (spiro-OMeTAD), the synthesis of which is complex and requires extensive, costly purification.[4] The spiro-OMeTAD HTM is usually deposited by spin coating, which typically incorporates only ca. 5% of the expensive starting material[5] and produces nonconformal films.[6] To compensate for this lack of conformality, a HTM of spiro-OMeTAD must be at least 150 nm thick to prevent shunting between the absorber and the back contact of the cell.[7] In contrast, inorganic HTMs can be deposited by vacuum techniques that require significantly less material to fully coat an underlying surface. Indeed, a solar cell with a power conversion efficiency greater than 10% can be produced using only 5 nm of an inorganic HTM.[8] It is clear that the current usage of a thick and prohibitively expensive organic HTM is far from ideal. The development of a suitable alternative to the spiro-OMeTAD HTM is imperative for the commercial development of perovskite photovoltaics.

One class of materials that might provide an inexpensive HTM is copper(I) halides. Cuprous iodide (CuI) has been used successfully in a perovskite solar cell,[9,10] with devices exhibiting power conversion efficiencies of up to 13.6%.[11] Cuprous bromide (CuBr) also shows promise: it is a p-type semiconductor with a hole concentration on the order of $10^{16}\,cm^{-3}$ and a hole mobility of $0.4\,cm^2\,V^{-1}\,s^{-1}$.[12] The p-type conductivity is thought to originate from copper vacancies and oxygen doping.[12] CuBr features a wide bandgap of 2.9 eV, which would prevent parasitic light absorption during use in a solar cell.[13] Films of CuBr have been deposited previously by vacuum evaporation,[14] molecular beam epitaxy,[15] and rf sputtering.[16]

Chemical vapor deposition (CVD) is a more appealing growth process for HTMs because it can produce films with high thickness uniformity and conformality over large areas of deposition. However, metal fluorides are the only halide compounds with known CVD growth processes.[17–19] Previous research in this lab indicates that direct CVD of metal halides is not well controlled when highly acidic hydrogen halide precursors (HX, with X = Cl, Br, I) are used. The reaction between HX and a metalorganic precursor does in fact produce the desired metal halide material by

[a)]R. Heasley and C. M. Chang contributed equally to this work.
[b)]Electronic mail: gordon@chemistry.harvard.edu

transferring a proton from HX to the anionic ligand of the metalorganic precursor, thereby releasing the neutral form of the ligand to be evacuated. However, CVD processes continuously supply both precursor vapors, allowing excess HX to protonate the newly released ligand a second time if that free ligand is basic. This acid–base reaction forms a ligand-hydrogen halide salt that is incorporated into the resultant film. For example, X-ray photoelectron spectroscopy (XPS) performed on nominal CuBr deposited by pulsed-CVD reveals carbon and nitrogen contamination consistent with the acetamidinium bromide salt (Fig. S1 in supplementary materials).[20]

Atomic layer deposition (ALD) is a type of CVD that separates the introduction of precursor vapors by purging with an inert gas and evacuating after each exposure. ALD is known as "self-limiting" because film growth proceeds by cycles of alternating precursor exposures and continues in each cycle only until surface reactive sites are depleted.[21] It seems plausible that pure metal halide films could be deposited by this method, given that the sequential nature of ALD would prevent the exposure of a basic ligand to a strong hydrogen halide acid. However, in an ideal ALD sequence, the hydrogen halide exposure step produces a halide-terminated surface, which means that no surface reactive sites are available for the next cycle of metalorganic precursor exposure. This limitation could be overcome if either the hydrogen halide or the metal precursor were able to adsorb to the film surface strongly enough to remain through the purge and evacuation steps. Previous research in this lab demonstrating the failure of ALD to produce any film under a variety of conditions indicates that this strong adsorption does not occur for the copper compound bis(*N*,*N*′-di-*sec*-butylacetamidinato)dicopper(I), $[Cu(sBu_2AMD)]_2$. With regard to hydrogen halides, it has been shown that strong adsorption on metal halide surfaces occurs only for HF, as a result of the formation of bifluoride (FHF^-) anions on the surface.[22] Adsorption of other hydrogen halides to a metal halide film is too weak to bind the molecule to the surface during purging and evacuation.[22] As such, we see no direct route to ALD of metal halides (with the exception of fluorides) using metalorganic precursors and hydrogen halide reactants.

Given the obstacles to the direct deposition of metal halides by CVD or ALD, the development of an alternative method for vapor deposition of CuBr and other halides is needed. Here, a novel route to the vapor deposition of pure CuBr by a two-step process is presented. A film of Cu_2S is first deposited by a pulsed-CVD reaction between $[Cu(sBu_2AMD)]_2$ and hydrogen sulfide.[23] This film is then exposed to anhydrous hydrogen bromide gas while held at a temperature of 60 °C. XPS reveals that the HBr exposure is able to fully convert at least 100 nm of the deposited Cu_2S to CuBr. Structural and morphological properties of the resultant CuBr films are presented and discussed.

II. EXPERIMENT

A. Film growth

Cu_2S and CuBr films were grown in a custom-built, hot-walled ALD reactor similar in design to those described in previous work.[24] Films were deposited on 1 × 1 in. substrates of Si with a 300-nm surface layer of SiO_2 grown by wet oxidation. Substrates were sequentially rinsed in semiconductor-grade acetone and isopropanol (BDH, ≥99%) and then dried in a nitrogen gas stream. The substrates were then treated with UV-ozone for 5 min to promote the formation of surface hydroxyl groups.

Thin films of Cu_2S were deposited via pulsed-CVD using exposures to $[Cu(sBu_2AMD)]_2$ (Dow Chemical Company, synthesis first reported by Li *et al.*[25]) and H_2S (Airgas, 4 wt. % in N_2). Both precursors were used as received, and the $[Cu(sBu_2AMD)]_2$ was loaded into a vacuum bubbler under a nitrogen atmosphere to prevent decomposition in air. The $[Cu(sBu_2AMD)]_2$ vapor was transferred to the reactor chamber by a purified nitrogen carrier gas held at a pressure of 10 Torr in the bubbler. The $[Cu(sBu_2AMD)]_2$ and H_2S/N_2 reactants were mixed together in a region 1 in. in length and 0.57 in. in diameter before reaching the substrate holder. Swagelok ALD valves operated by LABVIEW executed the pulsed-CVD recipes. Pulsed-CVD is similar to ALD, but omits the purging step between precursor doses. The timing sequence used for the Cu_2S recipe may be expressed as t_1-t_2-t_3-t_4-t_5, where t_1 is the exposure time of the $[Cu(sBu_2AMD)]_2$ precursor, t_2 is the exposure time of the H_2S/N_2 mixture, t_3 is a waiting period during which all valves are closed and deposition occurs, t_4 is the nitrogen purge time, and t_5 is the evacuation time, with all times given in seconds. The timing sequence was 1-1-30-10-30 for all Cu_2S depositions. $[Cu(sBu_2AMD)]_2$ was delivered at a partial pressure of 0.025 Torr for a total exposure of 0.85 Torr-s, and the H_2S/N_2 mixture was delivered at a pressure of 2.6 Torr for a total H_2S exposure of 3.2 Torr-s. The bubbler temperature of $[Cu(sBu_2AMD)]_2$ was maintained at 130 °C while the substrate temperature was varied from 100 to 200 °C. The inlet and outlet of the reactor tube furnace were heated to temperatures from 100 to 150 °C by Omega FGH heating tape regulated by an Omega miniature benchtop proportional-integral-derivative controller.

After completion of the Cu_2S deposition, the films were removed from the reactor, and the substrate temperature was adjusted to 30, 60, or 180 °C. Half of the as-deposited films were stored under N_2 atmosphere for future characterization and half were returned to the reactor after a brief (ca. 5 min) air exposure. At this point, conversion to CuBr proceeded via repeated exposures to anhydrous HBr (MilliporeSigma, ≥99%, used as received). The HBr was introduced by a 1-s pulse at a pressure of 1.3 Torr followed by a 30-s wait period with all valves closed. The total HBr exposure was 36 Torr-s. This was followed by a 10-s N_2 purge and 30-s evacuation. The repeated purging and evacuation steps were implemented to ensure the removal of generated H_2S and the continuation of the forward conversion reaction. The number of cycles was typically 484, which corresponds to about 4 h of total exposure to HBr. Although the films do not appear to oxidize or hydrolyze in air, all as-deposited and converted samples were stored under N_2 atmosphere except during analysis.

B. Film characterization

Electron microscopy and energy dispersive X-ray spectroscopy (EDS) were performed in a Zeiss Supra 55 scanning electron microscope (SEM). X-ray diffraction (XRD) patterns were recorded in a Bruker D2 PHASER X-ray diffractometer using Cu Kα radiation ($\lambda = 1.542$ Å) and a θ-2θ scan. XPS was performed on a Thermo Scientific K-Alpha spectrometer equipped with a monochromatized Al Kα X-ray source, 12 kV electron beam, and Ar^+ sputtering gun. Depth profiles were collected by sputtering at 500 eV for 50 s per level, unless otherwise stated. The XPS sputtering rate was determined by dividing the film thickness as determined by SEM by the total sputtering time before the SiO_2 substrate was detected.

III. RESULTS AND DISCUSSION

A. Cu_2S growth

The growth of Cu_2S was optimized across several variables with the ultimate goal of producing a pure, continuous film of uniform thickness. Pulsed-CVD was chosen as the deposition method for its accelerated growth rate relative to ALD.[26] XPS survey spectra reveal that depositions conducted between 120 and 180 °C produced films containing solely copper and sulfur, whereas films deposited at 100 or 200 °C also contain carbon (Fig. S2 in supplementary materials).[20] As evidenced by electron micrographs, growth proceeds by island coalescence. Figures 1(a)–1(c) compare pulsed-CVD Cu_2S films after 322 cycles of growth at 180, 150, and 120 °C, respectively. In these depositions, the temperature at the inlet of the reactor tube, ca. 1 in. from the substrate, was set to 150, 120, and 100 °C, respectively. As the progression from Fig. 1(a) to Fig. 1(c) shows, surface coverage increases as substrate and inlet temperatures decrease. Of particular significance is Fig. 1(c), which demonstrates that the reaction between $[Cu(sBu_2AMD)]_2$ and H_2S proceeds even at the low temperature of 120 °C. This high reactivity implies that if the inlet of the reactor tube is heated to 120 °C or greater, film deposition can occur in the mixing region before the precursors reach the substrate holder. As such, the observed reduction in surface coverage for higher growth temperatures likely results from significant film deposition in the mixing region, owing to the higher corresponding inlet temperature. Much of the delivered precursor is therefore consumed upstream of the SiO_2 substrates. The reaction proceeds more slowly at an inlet temperature of 100 °C, which limits the deposition in the mixing region and leads to higher surface coverage of Cu_2S at a substrate temperature of 120 °C. High-quality films of Cu_2S can also be grown more quickly at this temperature by pulsed-CVD with the waiting period $t_3 = 1$ s, as well as by standard ALD.

Figures 1(d) and 1(e) show the morphology of Cu_2S films deposited at 120 °C over 400 and 500 cycles, respectively. At this temperature, film closure occurs between 322 and 500 cycles, and the growth per cycle ranges from 1.1 to 1.7 Å/cycle, with the higher values calculated from thicker films. This large variation in growth per cycle at a single temperature is likely due to a relatively higher amount of film deposited per cycle during steady-state Cu_2S deposition as compared with initial nucleation. The existence of separate nucleation and bulk deposition growth regimes is relatively common in ALD and CVD processes.[27–30] Figure 1(f) is a high-resolution XPS spectrum of the Cu2p peak obtained after 45 s of Ar^+ sputtering. While C and O are detected at the surface of the deposited films, these contaminants are

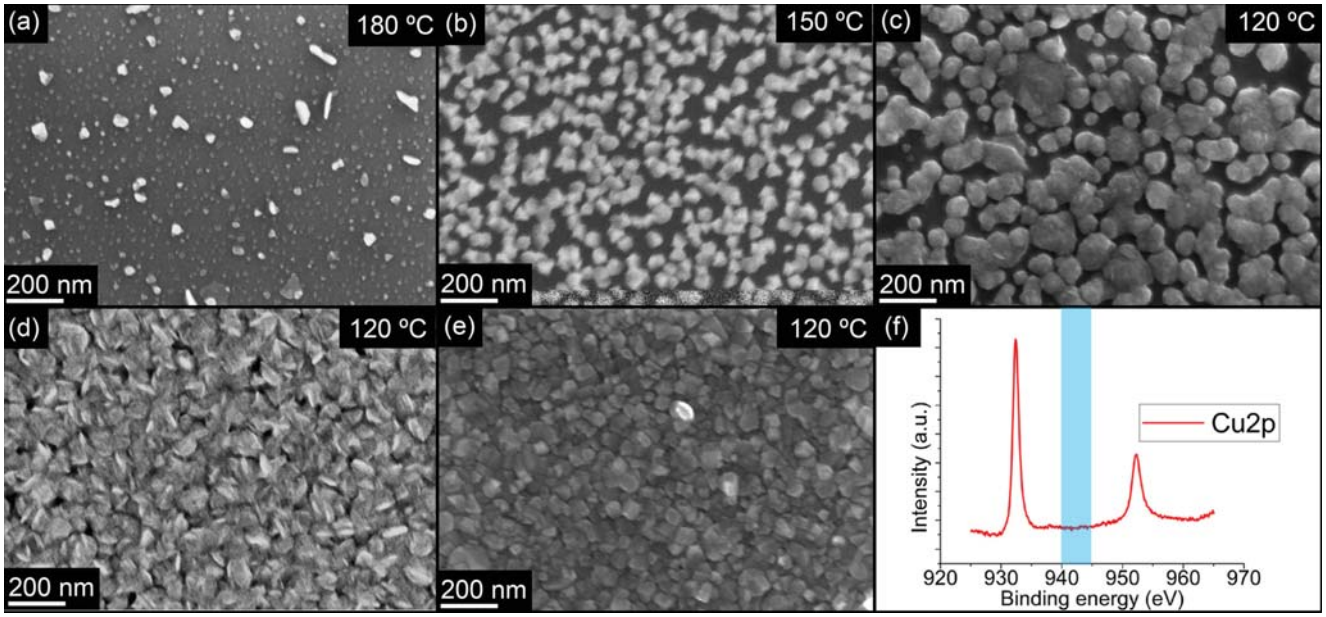

FIG. 1. (Color online) SEM images of Cu_2S film coverage after 322 cycles at a growth temperature of (a) 180, (b) 150, and (c) 120 °C. The substrate temperature of 120 °C was selected for its superior film coverage and Cu_2S films were deposited for (d) 400 and (e) 500 cycles. A high-resolution XPS scan of the Cu2p region shown in (f) gives no indication of the Cu^{2+} satellite peak typically observed at 943 eV (highlighted region).

removed after 45 s of Ar^+ sputtering and the absence of the characteristic Cu^{2+} satellite peak at 943 eV confirms copper is present as Cu^+ throughout the film.[31]

B. CuBr growth

After optimization of the Cu_2S growth process, experiments were conducted to convert the Cu_2S film to pure CuBr. The deposited films of Cu_2S were exposed to anhydrous HBr in accordance with the reaction

$$Cu_2S + 2\,HBr \rightleftharpoons 2\,CuBr + H_2S. \quad (1)$$

This reaction is thermodynamically favorable with a ΔG value of -40 kJ/mol at 60 °C (details of this calculation can be found in the supplementary materials).[20] Films of Cu_2S with a range of thicknesses from 60 to 400 nm were first prepared. These films were then heated to 60 °C and exposed to 484 pulses of HBr at a pressure of 1.3 Torr, amounting to a total exposure time of 4 h. The variation in atomic composition through the thickness of the converted films was measured by a depth profile within the XPS. Figure 2 shows the incomplete conversion of a 400-nm thick film of Cu_2S. As evidenced by the presence of Br, the HBr was able to penetrate through hundreds of nanometers of the film, fully converting the top 100 nm to CuBr (highlighted region). After this top 100 nm is removed by sputtering, sulfur becomes detectable by XPS and the film transitions gradually to predominantly Cu_2S. Oxygen and silicon from the SiO_2 substrate become visible after the full 400-nm thickness is removed. The forward reaction in Eq. (1) is slightly more exergonic at 30 °C ($\Delta G = -42$ kJ/mol) and does proceed, but the penetration depth of the HBr is shallower, with 9 h of exposure resulting in only 25 nm of CuBr at the surface (Fig. S3 in supplementary materials).[20]

Conversion of Cu_2S to CuBr is further evidenced by XRD analysis before and after HBr exposure. Figure 3 presents the diffractograms of the as-deposited Cu_2S film and the same film after a 4-h exposure to HBr at 60 °C. Figure 3(a) shows that the as-deposited Cu_2S films are crystalline and highly oriented. The experimental pattern best matches PDF

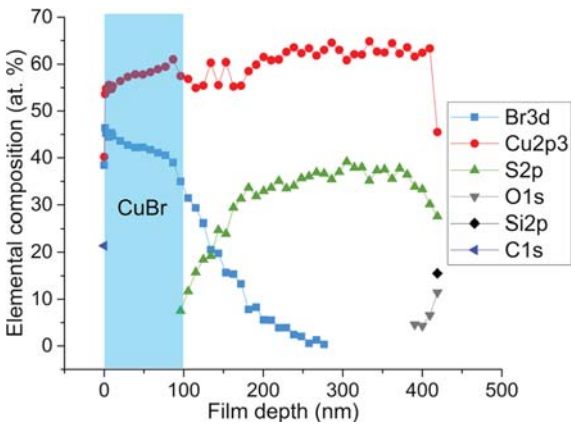

FIG. 2. (Color online) Depth profile obtained by XPS of a film converted from a 400-nm thick film of Cu_2S.

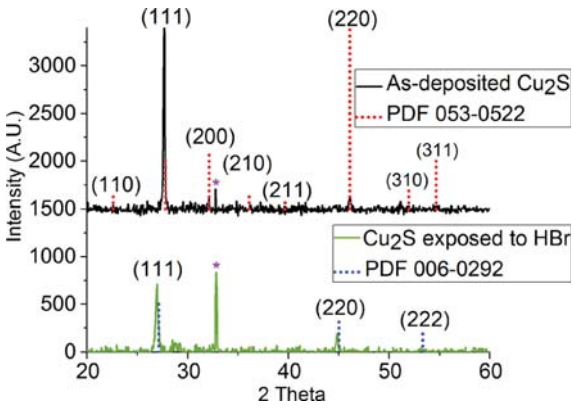

FIG. 3. (Color online) X-ray diffraction patterns of as-deposited 250 nm thick Cu_2S film (top) and the same film after conversion of the top 100 nm to CuBr via a 4-h exposure to HBr at 60 °C (bottom). The asterisk (*) denotes a background peak associated with the XRD instrument itself.

53-0522 for cubic Cu_2S, though the expected crystal structure for Cu_2S formed at 120 °C is the hexagonal high-chalcocite.[32] This discrepancy may be due to the significant impact of small deviations in stoichiometry on the resultant crystal structure of Cu_2S films, which complicates the precise crystallographic analysis of this material by XRD.[33] Figure 3(b) illustrates the measured XRD pattern of the same Cu_2S film following the HBr exposure, which matches PDF 006-0292 for γ-CuBr. Both the as-deposited and converted films appear to be (111)-oriented.

The film morphology was also influenced by the duration and temperature of the HBr exposures. HBr exposure tests were conducted at 30, 60, and 180 °C with a total exposure time of either 4 or 10 h. These two parameters control the extent of the conversion. The use of longer HBr exposures or higher reaction temperatures resulted in a greater volume of Cu_2S converted to CuBr. Electron micrographs in Fig. 4 show the variation in film morphology produced by these changes in exposure conditions. For shorter HBr exposure times or lower reaction temperatures, the converted CuBr formed as a surface layer that appeared rougher than the as-deposited Cu_2S, but remained continuous. However, for longer exposures or higher reaction temperatures, the conversion of Cu_2S progressed farther into the film and two distinct morphologies developed. The SEM image in Fig. 4(b) illustrates these morphologies. The upper layer is comprised of uncoalesced, 1 μm-sized grains, and the layer beneath is made up of 200-nm grains. Both layers are discontinuous, though the large grains of the top layer are more spatially separated than the smaller grains underneath. Figure 4(f) shows a similar discontinuous morphology, except the grains of the top layer are smaller. Two-dimensional EDS mapping shown in Fig. 5 confirms that the larger grains at the surface are composed of copper and bromine, whereas the smaller grains beneath are composed of copper and sulfur. The SiO_2 substrate is also visible through the converted film.

The thickness of the as-deposited Cu_2S affects the morphology of the converted CuBr. Figures 4(c) and 4(f) show films of Cu_2S with different initial thicknesses that have

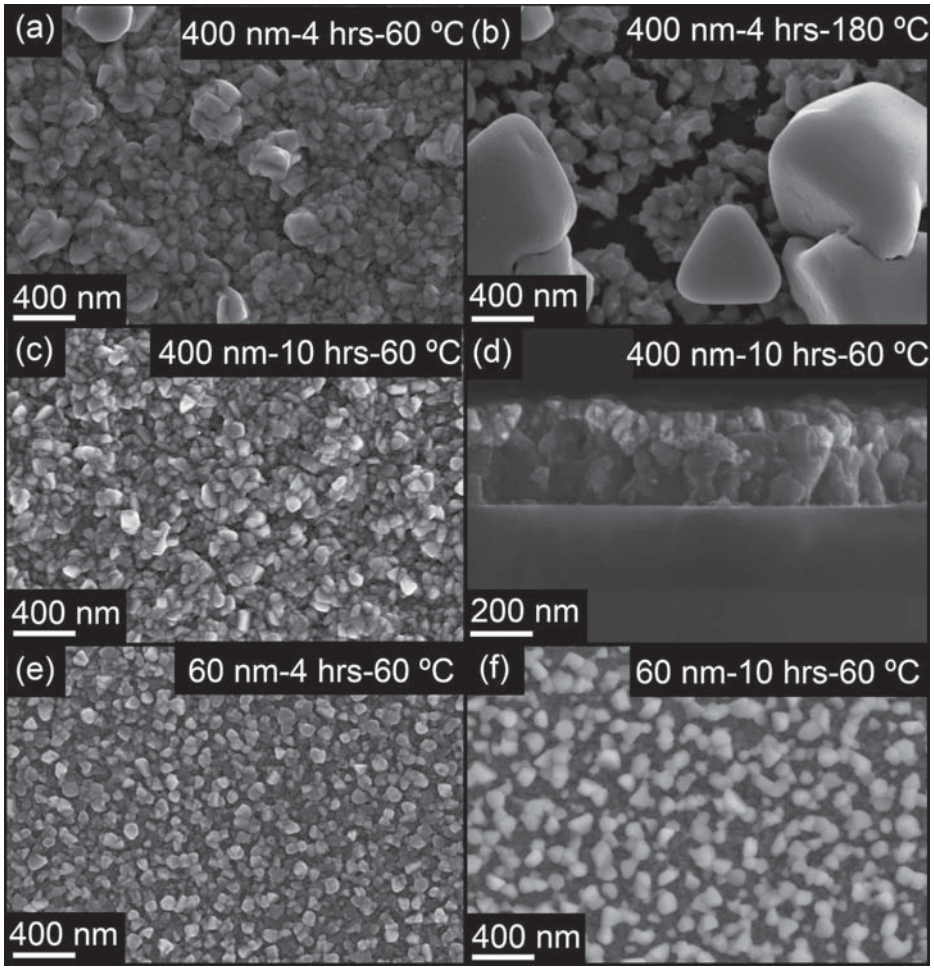

FIG. 4. SEM images of Cu_2S films with initial thickness x, exposed to HBr for y hours at a temperature of z °C (denoted x-y-z) (a) 400 nm-4 h-60 °C; (b) 400 nm-4 h-180 °C; (c) 400 nm-10 h-60 °C; (d) 400 nm-10 h-60 °C imaged in cross-section; (e) 60 nm-4 h-60 °C; and (f) 60 nm-10 h-60 °C.

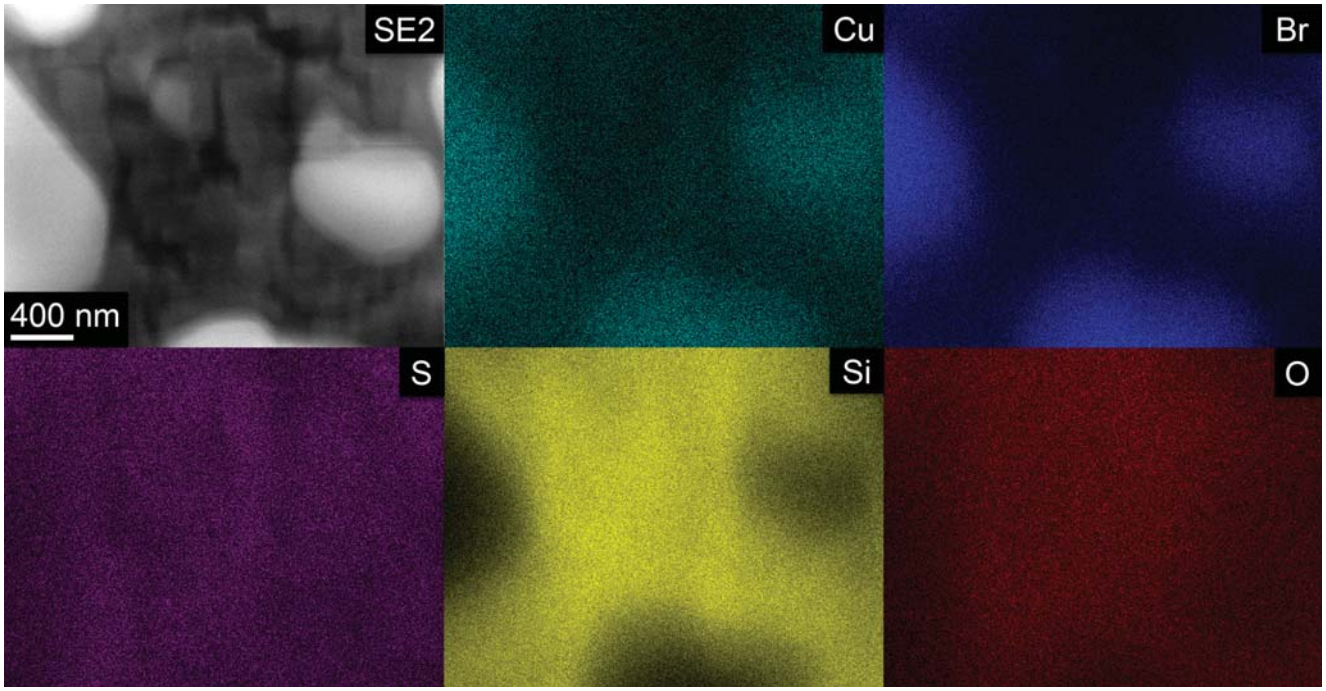

FIG. 5. (Color online) EDS composition mapping of a 400-nm thick film of Cu_2S exposed to HBr for 4 h at 180 °C.

TABLE I. As-deposited Cu_2S film thicknesses and subsequent HBr exposure parameters. Elemental composition was measured by XPS survey spectra after 30 s of Ar^+ sputtering.

As-deposited thickness (nm)	Exposure duration (h)	Exposure temperature (°C)	Cu (at. %)	Br (at. %)	S (at. %)	Si (at. %)	O (at. %)
400	4	60	54	46			
400	4	180	45	35	14	2.5	4.5
400	10	60	56	45			
60	4	60	54	46			
60	10	60	41	9	29	11	10

been exposed to HBr for 10 h at 60 °C. The 400-nm thick film of Fig. 4(c) has a smooth, continuous surface of CuBr [visible in cross-section in Fig. 4(d)], whereas the 60-nm thick film of Fig. 4(f) has developed the discontinuous morphology. Table I contains the atomic composition of the films imaged in Fig. 4 as determined by XPS survey spectra conducted after 30 s of Ar^+ sputtering. The surface of the film imaged in Fig. 4(c) is exclusively composed of copper and bromine, whereas for the film in Fig. 4(f), copper and bromine are detected, but also sulfur and the silicon and oxygen of the SiO_2 substrate. From these results, it appears that the conversion of Cu_2S to CuBr upon exposure to HBr proceeds until enough of the Cu_2S is consumed that the SiO_2 surface is exposed. At this point, the CuBr agglomerates into larger grains on the surface of the remaining Cu_2S. This result suggests that the surface energy of the partially converted film is minimized when CuBr-Cu_2S and CuBr-CuBr interactions are favored over CuBr-SiO_2 interactions. Thinner as-deposited films of Cu_2S require shorter HBr exposures and lower reaction temperatures to develop the discontinuous morphology, which is consistent with this hypothesis, as there is less Cu_2S to convert before the SiO_2 surface is exposed. Research is ongoing to find a substrate that will allow a film of Cu_2S to be converted completely to a thin, continuous film of CuBr.

IV. SUMMARY AND CONCLUSIONS

Thin films of CuBr were deposited by a two-step process, starting with the growth of Cu_2S by pulsed-CVD of bis(*N*,*N*′-di-*sec*-butylacetamidinato)dicopper(I) and hydrogen sulfide at temperatures ranging from 100 to 200 °C. A growth temperature of 120 °C produced crystalline Cu_2S films with carbon and oxygen contents below the detection limit of XPS. These Cu_2S films were then converted to CuBr by exposure to anhydrous hydrogen bromide at 60 °C. The reaction produced films of pure, crystalline (111)-oriented γ-CuBr. The morphology of the resultant CuBr was dependent on the proximity of the growth front to the SiO_2 substrate, with much larger grains forming in a discontinuous arrangement when the substrate was exposed. This sulfide-to-bromide conversion process is in principle generalizable to the preparation of halides of many different metals, thereby extending the potential scope of halide CVD beyond solely metal fluorides.

ACKNOWLEDGMENTS

The authors gratefully acknowledge support from the EPA Marshall Scholarship (to C. M. Chang) and the Center for Excellence in Education Research Science Institute (to K. Liu). This work was performed in part at the Center for Nanoscale Systems (CNS), a member of the National Nanotechnology Coordinated Infrastructure Network, which is supported by the National Science Foundation under NSF Award No. 1541959. CNS is part of Harvard University. Xiabing Lou provided valuable assistance in XRD analysis.

[1]A. Kojima, K. Teshima, Y. Shirai, and T. Miyasaka, J. Am. Chem. Soc. **131**, 6050 (2009).
[2]NREL, "Best research-cell efficiencies," 2016, http://www.nrel.gov/pv/assets/images/efficiency_chart.jpg.
[3]K. Rakstys, M. Saliba, P. Gao, P. Gratia, E. Kamarauskas, S. Paek, V. Jankauskas, and M. K. Nazeeruddin, Angew. Chem. Int. Ed. **55**, 7464 (2016).
[4]M. Saliba *et al.*, Nat. Energy **1**, 15017 (2016).
[5]S.-R. Tseng, H.-F. Meng, K.-C. Lee, and S.-F. Horng, Appl. Phys. Lett. **93**, 153308 (2008).
[6]E. Yenilmez, Q. Wang, R. J. Chen, D. Wang, and H. Dai, Appl. Phys. Lett. **80**, 2225 (2002).
[7]G.-W. Kim, D. V. Shinde, and T. Park, RSC Adv. **5**, 99356 (2015).
[8]W. Yu *et al.*, Nanoscale **8**, 6173 (2016).
[9]J. A. Christians, R. C. M. Fung, and P. V. Kamat, J. Am. Chem. Soc. **136**, 758 (2014).
[10]G. A. Sepalage, S. Meyer, A. Pascoe, A. D. Scully, F. Huang, U. Bach, Y.-B. Cheng, and L. Spiccia, Adv. Funct. Mater. **25**, 5650 (2015).
[11]W.-Y. Chen, L.-L. Deng, S.-M. Dai, X. Wang, C.-B. Tian, X.-X. Zhan, S.-Y. Xie, R.-B. Huang, and L.-S. Zheng, J. Mater. Chem. A **3**, 19353 (2015).
[12]P. Knauth, Y. Massiani, and M. Pasquinelli, Phys. Status Solidi A **165**, 461 (1998).
[13]M. Altarawneh, A. Marashdeh, and B. Z. Dlugogorski, Phys. Chem. Chem. Phys. **17**, 9341 (2015).
[14]A. Cowley, F. O. Lucas, E. Gudimenko, M. M. Alam, D. Danieluk, A. L. Bradley, and P. J. McNally, J. Phys. D: Appl. Phys. **43**, 165101 (2010).
[15]A. Yanase and Y. Segawa, Surf. Sci. **329**, 219 (1995).
[16]J.-L. Seguin, M. Bendahan, G. Lollmun, M. Pasquinelli, and P. Knauth, Thin Solid Films **323**, 31 (1998).
[17]T. Pilvi, M. Ritala, M. Leskelä, M. Bischoff, U. Kaiser, and N. Kaiser, Appl. Opt. **47**, C271 (2008).
[18]M. Mäntymäki, J. Hämäläinen, E. Puukilainen, T. Sajavaara, M. Ritala, and M. Leskelä, Chem. Mater. **25**, 1656 (2013).
[19]Y. Lee, J. W. DuMont, A. S. Cavanagh, and S. M. George, J. Phys. Chem. C **119**, 14185 (2015).
[20]See supplementary materials at http://dx.doi.org/10.1116/1.4967726 for hypothesized reaction mechanism for *direct* p-CVD of CuBr, elemental composition of nominal CuBr film containing acetamidinium bromide salt, elemental compositions of Cu_2S films deposited at 100 and 200 °C, thermodynamic favorability calculations of the conversion reaction, and a depth profile of a 200-nm film of Cu_2S exposed to HBr for 9 h at 30 °C.
[21]S. M. George, Chem. Rev. **110**, 111 (2010).
[22]R. St. C. Smart, and N. Sheppard, Proc. Roy. Soc. London, A **320**, 417 (1971).
[23]A. B. F. Martinson, J. W. Elam, and M. J. Pellin, Appl. Phys. Lett. **94**, 123107 (2009).
[24]D. M. Hausmann, P. de Rouffignac, A. Smith, R. G. Gordon, and D. Monsma, Thin Solid Films **443**, 1 (2003).
[25]Z. Li, S. T. Barry, and R. G. Gordon, Inorg. Chem. **44**, 1728 (2005).
[26]P. Sinsermsuksakul, R. Chakraborty, S. B. Kim, S. M. Heald, T. Buonassisi, and R. G. Gordon, Chem. Mater. **24**, 4556 (2012).
[27]L. Baker, A. S. Cavanagh, D. Seghete, S. M. George, A. J. M. Mackus, W. M. M. Kessels, Z. Y. Liu, and F. T. Wager, J. Appl. Phys. **109**, 084333 (2011).
[28]Q. Ma, F. Zaera, and R. G. Gordon, J. Vac. Sci. Technol., A **30**, 01A114 (2012).

[29]D.-W. Choi, M. Yoo, H. M. Lee, J. Park, H. Y. Kim, and J.-S. Park, ACS Appl. Mater. Interfaces **8**, 12263 (2016).
[30]J. Lee, B. Hong, R. Messier, and R. W. Collins, Appl. Phys. Lett. **69**, 1716 (1996).
[31]E. Cano, C. L. Torres, and J. M. Bastidas, Mater. Corros. **52**, 667 (2001).
[32]A. B. F. Martinson, S. C. Riha, E. Thimsen, J. W. Elam, and M. J. Pellin, Energy Environ. Sci. **6**, 1868 (2013).
[33]*Non-Tetrahedrally Bonded Elements and Binary Compounds I*, Landolt-Börnstein–Group III Condensed Matter Vol. 41C, edited by O. Madelung, U. Rössler, and M. Schulz (Springer-Verlag, Heidelberg, 1998).